Effect of hidden geometry and higher-order interactions on the synchronization and hysteresis behavior of phase oscillators on 5-clique simplicial assemblies

Samir Sahoo [1,2] Bosiljka Tadić [3,4] Malayaja Chutani [5] and Neelima Gupte [5,2]

[1] *Department of Applied Mechanics, Indian Institute of Technology Madras, Chennai 600036, India*

[2] *Center for Complex Systems & Dynamics, Indian Institute of Technology Madras, Chennai 600036, India*

[3] *Department of Theoretical Physics, Jožef Stefan Institute, Jamova 39, Ljubljana, Slovenia*

[4] *Complexity Science Hub, Josephstaedterstrasse 39, Vienna, Austria*

[5] *Department of Physics, Indian Institute of Technology Madras, Chennai 600036, India*

(Received 22 May 2023; accepted 1 September 2023; published 25 September 2023)

The hidden geometry of simplicial complexes can influence the collective dynamics of nodes in different ways depending on the simplex-based interactions of various orders and competition between local and global structural features. We study a system of phase oscillators attached to nodes of four-dimensional simplicial complexes and interacting via positive/negative edges-based pairwise K_1 and triangle-based triple $K_2 \geqslant 0$ couplings. Three prototypal simplicial complexes are grown by aggregation of 5-cliques, controlled by the chemical affinity parameter ν, resulting in sparse, mixed, and compact architecture, all of which have 1-hyperbolic graphs but different spectral dimensions. By changing the interaction strength $K_1 \in [-4, 2]$ along the forward and backward sweeps, we numerically determine individual phases of each oscillator and a global order parameter to measure the level of synchronization. Our results reveal how different architectures of simplicial complexes, in conjunction with the interactions and internal-frequency distributions, impact the shape of the hysteresis loop and lead to patterns of locally synchronized groups that hinder global network synchronization. Remarkably, these groups are differently affected by the size of the shared faces between neighboring 5-cliques and the presence of higher-order interactions. At $K_1 < 0$, partial synchronization is much higher in the compact community than in the assemblies of cliques sharing single nodes, at least occasionally. These structures also partially desynchronize at a lower triangle-based coupling K_2 than the compact assembly. Broadening of the internal frequency distribution gradually reduces the synchronization level in the mixed and sparse communities, even at positive pairwise couplings. The order-parameter fluctuations in these partially synchronized states are quasicyclical with higher harmonics, described by multifractal analysis and broad singularity spectra.

DOI: 10.1103/PhysRevE.108.034309

I. INTRODUCTION

Mapping complex systems onto networks that embody functional connections among the systems' constitutive elements often involves higher-order couplings, which induces more complex geometries. Identifying these hidden geometry features of various orders and assessing their impact on system dynamics is currently a focus of network theory [1–3] and its applications, from the brain [4–9], to large-scale social systems and emergent networks [10–13], to materials design [14–16]. These complex topologies can be described by algebraic topology [17,18] with identifying full graphs (cliques) of all sizes that are present as well as the faces that they share with other cliques to make the actual simplicial complex. In this context, the underlying network (1-skeleton of the simplicial complex) is made of the edges connecting two nodes, which may appear as faces of the order 1 of larger simplexes (triangles, tetrahedrons, etc.).

In the theory of complexity, the emergence of new features at a larger scale, as a key property of a complex system, can be associated with the collective dynamic fluctuations. Such dynamic phenomena, through interactions among dynamical units, appear with long-range spatiotemporal correlations that are characteristics of critical states, either with a dynamical phase transition or as self-organized critical attractors in driven nonlinear dynamics; see a brief survey in [19] and references therein. The underlying simplicial structure can provide multiple interactions among dynamical units associated with the network nodes. In particular, pairwise interactions occur along the network's edges; meanwhile, higher interactions can be geometrically embedded into the triangles, tetrahedrons, and higher faces up to the largest simplex found in the structure. The two leading (i.e., pairwise and triangle-based) interactions are expected to impact the collective dynamics critically, given the renormalization-group theory [20,21]; however, this question remains open in finite systems and complex geometries. The actual impact of these interactions also depends on the type of the dynamics of interacting units. For example, the higher-order interactions, e.g., within large cliques, may enable the fast spreading of diseases [22] and enhance traveling waves in networks of neurons but without pathological full synchronized states [23,24]. On the other hand, the triangle-based couplings induce geometric frustration with long-range effects in spin kinetics [25–27].

Phase synchronization among many interacting units is a prototypal nonlinear dynamics model to study the cooperative phenomena in many complex systems, including applications in neuroscience, engineering, etc. [28–30]. Current research on the influence of higher-order coupling on synchronization processes is focused on the following: (i) searching for conditions of perfect synchronization among oscillators on nodes of general networks in the presence of a p-point interactions [31]; (ii) searching for conditions for full synchronization between topological signals associated with simplexes of different order (see the recent work in Ref. [32] and references there); and (iii) understanding the nature of synchronization-desynchronization processes of the oscillators at nodes of simplicial complexes with geometric interactions embedded into simplex faces of different order [33–37]. Our work belongs in the third category. In this context, key questions concern the emergence and disappearance of collective dynamic behavior, measured by the order parameter on the hysteresis loop, when the strengths of the various interactions embedded in the geometry vary. For example, the presence of triangle-based interactions is understood to disrupt the order promoted by increasing the strength of pairwise couplings, and it can cause sudden desynchronization [33,36,38]. Furthermore, the occurrence of *partially synchronized* phases with negative pair interactions is another striking feature of geometric interactions on simplicial complexes; see, for example, Ref. [36] and references therein. As a special case, the frustrated synchronization [39] is often attributed to complex structures, e.g., in brain networks, where higher geometries are expected to play an important role [23,24,37]. Theoretically, the influence of topology on diffusive processes can be captured to a good extent by spectral analysis of the network [38,40–43]. A suitable measure is the spectral dimension d_s derived from the eigenvalue spectrum of the Laplace operator associated with the network adjacency matrix; higher-order combinatorial Laplacians [44] are adequate for the diffusion of topological signals on simplicial complexes; see [32]. In the context of phase synchronization, it has been understood [38] that networks with $d_s \geqslant 4$ enable the thermodynamically stable global synchronization; meanwhile, for $d_s \in (2, 4]$ an entrained synchronization phase can be observed, and the correlations among the nearest phases become unstable when $d_s \lesssim 2$ in the limit $N \to \infty$. Considering the systems with complex geometry, the following issues need to be better understood: (a) Unlike global synchronization, where conditions can be formulated analytically, as mentioned above [31,32], the origin of *partial synchronization on simplicial complexes* and the nature of the underlying dynamical states is more elusive. (b) In addition to the topological dimension of a simplicial complex, the role of its architecture in synchronization processes remains to be clarified, especially concerning higher-order interactions and the internal inhomogeneity of the nodes' dynamics.

In this work, we tackle these questions by studying the synchronization and desynchronization processes on several four-dimensional simplicial complexes of a controlled architecture, all assembled by 5-cliques as building blocks. Building on our previous work [36], we consider the phase synchronization of Kuramoto oscillators on the nodes interacting via simplex-embedded interactions; we expand the study in several directions. More precisely, our aims are (i) to investigate the role of the architecture of simplicial complexes while keeping their topological dimension and size fixed, and (ii) to reveal the conditions for partial synchronization in different architectures and examine the nature of fluctuations that sustain these partially ordered states. For this purpose, we grow three assemblies of 5-cliques by changing a controlled parameter in the model previously introduced in [15]; as explained in detail in the following section, these assemblies differ considerably in their architecture of simplexes and also have different spectral dimensions [42]. To investigate the network's ability to synchronize, i.e., by increasing the leading pairwise couplings and sustaining the reached state when the coupling strength is reduced, we track the hysteresis loop branches by varying the strength of the pairwise interaction in a large region from negative to positive values and back; meanwhile, we keep the three-phase couplings embedded into triangles of the actual complex and the distribution of internal frequencies fixed. Our analysis revealed how the network's ability to reach complete synchrony at the positive pairwise couplings and partial synchrony and incomplete desynchronization by negative interactions depends on the simplicial architecture corroborated with the distribution of internal frequencies. Remarkably, the level of partial synchronization at large negative pairwise couplings can be associated with the minimal size of the faces shared among neighboring 5-cliques, and it is virtually independent of the presence of higher-order interactions and the actual frequency distribution. The multifractal fluctuations of the order parameter are associated with these partially synchronized states emerging through roughly synchronized small clusters.

In Sec. II, we present three considered simplicial complexes and their structural features relevant to this work. Section III A introduces the dynamical model with the leading pairwise and triangle-based interactions on these complexes; then in Secs. III B, III C, and III D, we give the results regarding the hysteresis properties and individual phase evolution patterns. In Sec. IV, we present the multifractal analysis of the order-parameter fluctuations in two representative points of the hysteresis loop. Section V is devoted to a summary and a discussion of the results.

II. STRUCTURE OF THE 5-CLIQUE AGGREGATES WITH DIFFERENT SPECTRAL DIMENSION

To grow the four-dimensional simplicial complexes for our study, we use the generative model introduced in [15,45] for a cooperative self-assembly [14,46] of preformatted groups of nanoparticles. As explained in the Introduction, we fix the size of the building blocks as 5-cliques; starting from a single 5-clique, at each growth step a new clique is attached to the growing structure such that it shares one of its geometrical faces with a clique that is already present in the structure. In the present case, the possible faces are subcliques of the size $s = 1$, 2, 3, and 4, respectively, a single node, a link with two adjacent nodes, a triangle with three connected nodes, or a tetrahedron consisting of four nodes. What face would be shared is determined by the geometric compatibility factor and the chemical affinity parameter ν; see Ref. [15] for a

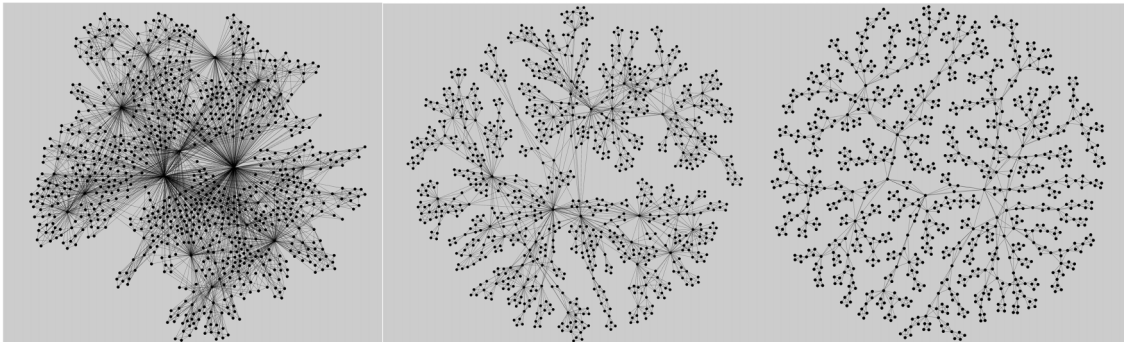

FIG. 1. Networks of 5-cliques grown by the self-assembly rules described in [15] observing the geometric compatibility for different chemical potential, left to right: $\nu = 5$ (compact), $\nu = 0$ (mixed), and $\nu = -5$ (sparse structure). Adding 5-cliques is stopped when the number of nodes reaches $N \geqslant 1000$.

detailed description, and Ref. [16] for an extended model with defect cliques. Specifically, the probability of sharing a face of the size s is given by

$$P(s_{\max}, s; t) = \frac{c_s(t)e^{-\nu(s_{\max}-s)}}{\sum_{s=1}^{s_{\max}-1} c_s(t)e^{-\nu(s_{\max}-s)}}, \tag{1}$$

where $c_s(t)$ stands for the number of geometrically compatible locations on the entire structure at the moment t where docking a simplex of the size s can be done. Note that, in the present case, we have $s_{\max} = 5$ fixed. The geometric factor is weighted by the chemical affinity ν [15] towards new $s_{\max} - s$ nodes that must be added to the structure after the face with s nodes is shared with a previous clique. Hence, for a large $\nu > 0$, sharing a maximal subclique (a tetrahedron) is favored, the emergent structure is compact, whereas when $\nu < 0$, the probability of adding more nodes is increasing. Thus, for a large negative ν, the cliques preferably share a single node (minimal face), resulting in a sparse structure. Without a chemical affinity factor, $\nu = 0$, sharing of faces of any size $s = 1, \ldots, 4$ can occur, subject to the geometric compatibility factors alone. The resulting structures that we use here are for $\nu = -5$, 0, and $+5$, shown in Fig. 1.

The structure of these simplicial complexes is characterized by several quantities, cf. Fig. 2, which are relevant to the present study. In particular, we determine the generalized-degree distributions $P(k_\mu)$, where k_μ (for $\mu = 2, 3, 4, 5$) indicates the number of edges, triangles, tetrahedra, and 5-cliques attached to a node, shown in Figs. 2(a)–2(d). In each panel, three lines/symbols stand for three architectures of Fig. 1. The three structures differ significantly in all of these distributions. In particular, the nodes in the compact simplicial complex (at $\nu = +5$) share a large number of simplexes of all orders, which leads to a distorted power-law distribution at high k_μ; meanwhile, the distributions of the structure at $\nu = 0$ with the same number of nodes are nearly power-law with a (finite-size) cutoff. On the other hand, the sparse system, grown with $\nu = -5$, exhibits a fast decaying exponential distribution for all simplex sizes.

The other measures are compatible with these features, shown in Figs. 2(e)–2(h). Specifically, the number of simplexes and faces of different sizes that are present in each simplicial structure, f_s, shown in Fig. 2(g), indicates that the compact simplicial complex at $\nu = +5$ possesses the largest number of triangles, and gradually the number of cliques of other sizes, compared to the structure for $\nu = 0$ and -5. The underlying network (1-skeleton of these simplicial complexes) exhibits some other properties that strongly vary with ν. In particular, these are the distributions of the shortest-path distances on the underlying graph, shown in Fig. 2(e), and the spectral dimension, which is determined for these graphs in Ref. [42], shown in Fig. 2(h). The spectral dimension for these three representative structures varies, in particular, $d_s = 1.57$, 2.11, and 4.01 for $\nu = -5$, 0, and 5, respectively; they are indicated by different symbols on the line $d_s(\nu)$, which is determined from the Laplacian eigenvalues distribution in [42] for a range of such structures. Similarly, the distributions on these networks, cf. Fig. 2(e), show that small distances prevail in the compact structure for $\nu = 5$, peaking at $d_{\max} = 3$, whereas the peak moves towards larger distances, i.e., $d_{\max} = 5$ and 10 for $\nu = 0$ and -5, respectively. On the other hand, these graphs are 1-hyperbolic by construction; see the discussion in the original work [15]. Specifically, because the cliques (which are $\delta_0 = 0$-hyperbolic objects) always share their faces in these structures, the hyperbolicity of the emergent complex is given [47,48] by $\delta_0 + 1$. Figure 2(f) demonstrates this by numerically computing the Gromov hyperbolicity parameter $\delta_{\max}$, which does not exceed 1 considering 10^9 different 4-tuples on these networks.

III. PHASE SYNCHRONIZATION ON FOUR-DIMENSIONAL SIMPLICIAL COMPLEXES

A. Dynamical model and simulations

We consider an ensemble of N coupled Kuramoto oscillators [30] associated with the nodes of a given simplicial complex. The equation governing the evolution of the phase angle θ_i of the ith oscillator is given by [36]

$$\dot{\theta}_i = \omega_i + \frac{K_1}{k_i^{(1)}} \sum_{j=1}^{N} A_{ij} \sin(\theta_j - \theta_i) + \frac{K_2}{2k_i^{(2)}} \sum_{j=1}^{N} \sum_{l=1}^{N} B_{ijl} \sin(\theta_j + \theta_l - 2\theta_i), \tag{2}$$

where ω's are the intrinsic frequencies of the phase oscillators. The second and third terms in Eq. (2) represent 1-simplex

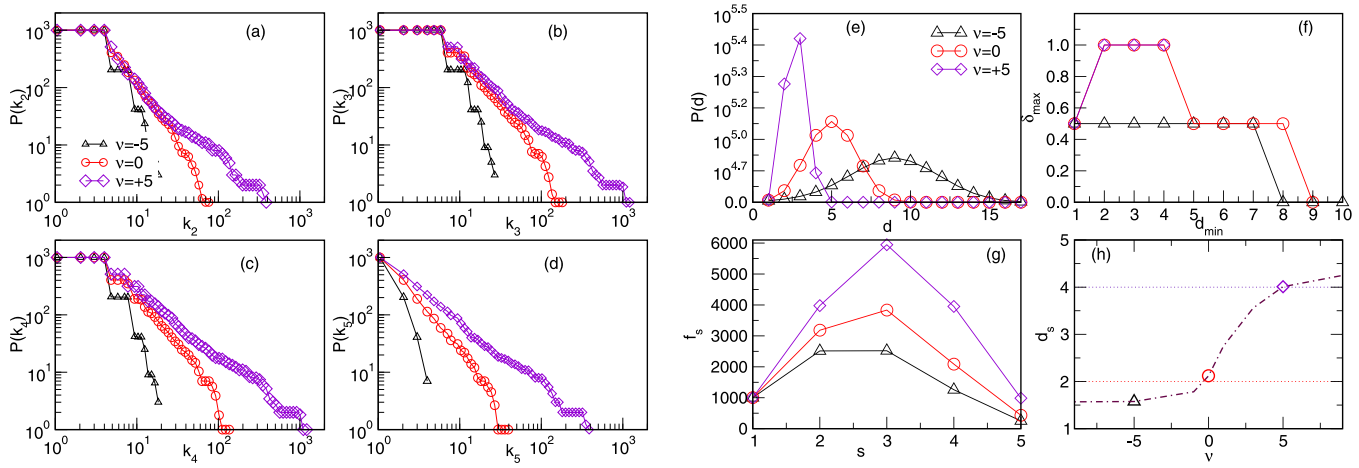

FIG. 2. Cumulative distributions of the generalized degree for the number of (a) links, (b) triangles, (c) tetrahedra, and (d) 5-cliques per node in three networks for different ν, as indicated in the unique legend. (e) The distribution of the shortest-path distances between node pairs, $P(d)$, vs the distance d; (f) the hyperbolicity parameter $\delta_{\max}$ vs the smallest distance $d_{\min}$ of the nodes 4-tuples on these three networks; (g) the number of simplexes f_s of different size s in them; and (h) the network's spectral dimension d_s for different ν. The same legend applies to all panels. The data in panel (h) are from Ref. [42].

and 2-simplex interactions, respectively. Note that three-node interactions of the ith oscillator are based on each 2-simplex (triangle) incident on node i, thus introducing a natural generalization of the pairwise interaction term [35]. Here, A_{ij} is an element of the 1-simplex adjacency matrix $\mathbf{A}$, such that $A_{ij} = 1$ if nodes i, j are connected by a link and 0 otherwise. In the second term, B_{ijl} is an element of the 2-simplex adjacency tensor $\mathbf{B}$, such that $B_{ijl} = 1$ if nodes i, j, l belong to a common 2-simplex (triangle) and 0 otherwise. Likewise, the normalization factors $k_i^{(1)}$ and $k_i^{(2)}$ indicate the number of links and triangles of the node i, respectively; cf. Fig. 2 for the structure of the actual simplicial complexes. The well-known Kuramoto order parameter can effectively quantify the degree of synchronization of the network,

$$r = \left\langle \left| \frac{1}{N} \sum_{j=1}^{N} e^{i\theta_j} \right| \right\rangle, \tag{3}$$

where the brackets $\langle \cdot \rangle$ indicate the time average.

In the simulations, for each network node $i = 1, 2, \ldots, N$, where we have $N = 1000$, 1002, and 1003 corresponding to $\nu = 5$, 0, and -5 networks, respectively, the initial conditions for θ_i are chosen randomly in the range $\theta_i \in [0, 2\pi]$. The numerical solution for the set of Eqs. (2) is performed using a numerical integration algorithm ODEINT from Python SciPy library [49]. For each set of parameter values, the system is iterated for 50 000 steps, with the time step $dt = 0.01$ and always considering the previous state of each dynamical variable; the procedure known as tracking the attractor [50] is used in most hysteresis studies. The order parameter in Eq. (3) is calculated in the asymptotic range considering the last 20 000 iterations. Further, to study the hysteresis properties, we track the system's trajectory as the coupling parameter K_1 is first adiabatically increased in steps $dK_1 = 0.1$ in the appropriate range from negative to positive values, typically $K_1 \in [-2, +2]$, constituting the forward sweep, and then decreased along the backward branch. Meanwhile, the strength of the higher-order interaction K_2 is kept fixed, and the internal frequencies of the oscillators ω_i are drawn from a given distribution, as explained below.

B. Partial synchronization at $K_1 < 0$: Hysteresis loop for uniform internal frequencies

In this section, we study an hysteresis loop for the interactions embedded in simplexes of different architectures described in Sec. II, when the internal frequencies of all oscillators are equal, i.e., $\omega \approx 1.0$ drawn from a δ-function distribution. In this way, we expect that the impact of the structure and related interactions will be more pronounced. As described above in Sec. III A, for a given value of K_2 and varying the pairwise coupling strength $K_1 \in [-5, +2]$ in small steps, the order parameter is computed first along the forward branch, and then back. The resulting hysteresis loops for the three networks of Fig. 1, and fixing K_2 to several representatives values between $K_2 = 0.0$ and 1.0, are summarized in Fig. 3.

As Fig. 3 shows, even though the internal frequencies of the oscillators are equal at all nodes, the shape of the hysteresis loop is significantly dependent on on the structure of the underlying simplicial complexes. On the forward sweep, by keeping $K_2 = 0$, we note the occurrence of partial synchronization at negative K_1 values, where the order parameter reaches $r \approx 0.5$, for the compact simplicial complex for $\nu = 5$. In the other two networks ($\nu = 0$ and -5), a much smaller but nonzero (within numerical error bars) value $r \approx 0.03$ is observed. Further increasing $K_1 > 0$, a smooth transition to a complete synchronization with $r \approx 1$ occurs in all networks.

On the backward sweep, the synchronized state persists until the negative pairwise or additional triangle interactions become strong enough to break the local order and spread throughout the system. The loop does not close even at very large negative K_1 unless the higher-order coupling of a given strength $K_2 > 0$ is applied; moreover, the needed higher-order interaction correlates with the network's compactness. Specifically, in the compact network ($\nu = 5$), cf. the bottom left

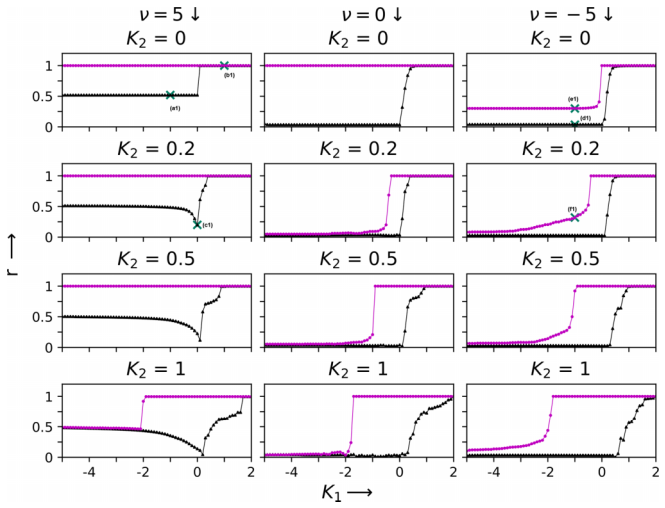

FIG. 3. Hysteresis sweep of the order parameter r as a function of 1-simplex coupling strength K_1 at different 2-simplex coupling strength K_2; the three vertical columns (from left to right) correspond to three simplicial complexes in Fig. 1 grown with the chemical affinity $\nu = 5$, 0, and -5, respectively. The solid triangles (black) and solid circles (magenta) refer to forward and backward sweeps, respectively. The intrinsic frequencies $\omega_i \approx 1.0$ at all nodes. The phase evolution patterns analyzed in the following section, Figs. 4(a1)–4(f1), correspond to the points marked on the hysteresis loop.

panel, the loop closes for $K_2 = 1.0$ via sudden desynchronization, in agreement with previous studies [33–36]. However, for $\nu = -5$, an incomplete abrupt desynchronization occurs even at $K_2 = 0.0$. Still, the loop closes gradually, reaching the forward branch for more negative K_1 values, cf. the top right panel and the panels below it. In the intermediate case, $\nu = 0$, a small $K_2 = 0.2$ suffices to induce an incomplete desynchronization, and the loop gradually closes at more negative K_1 values. By increasing the triangle-based coupling K_2, the apparent broadening of the loop superimposes these features in each particular network. It is also accompanied by the slower loop reaching full synchrony even at high positive pairwise couplings. In the following, we will focus on the evolution of the phases of all oscillators at specific values (K_1, K_2) on the hysteresis loop.

C. The dynamics of individual nodes and patterns behind partial synchronization

The global order parameter r discussed above quantifies the extent to which the oscillators are synchronized at a given set of parameter values. To get a deeper insight into the synchronization and desynchronization processes and their dependence on network geometry and interactions, we study the global phase angle $\theta_{\rm av}(t) = \sum_i \theta_i(t)/N$ as a function of time, the evolution of phase angles of each node, and the distribution of phase angles at a particular time; cf. Fig. 4.

The phase trajectories of individual nodes are shown in the top row of Figs. 4(a1)–4(f1); they are taken at corresponding points marked by crosses on the hysteresis loops in Fig. 3. In particular, these points correspond to the values of the two interactions $(K_1, K_2)f$, b on the forward f or backward b hysteresis branch, which are $(-1, 0)f$, $(-1, 0)b$, and $(0, 0.2)f$ for the compact network $\nu = 5$, patterns (a1), (b1), and (c1),

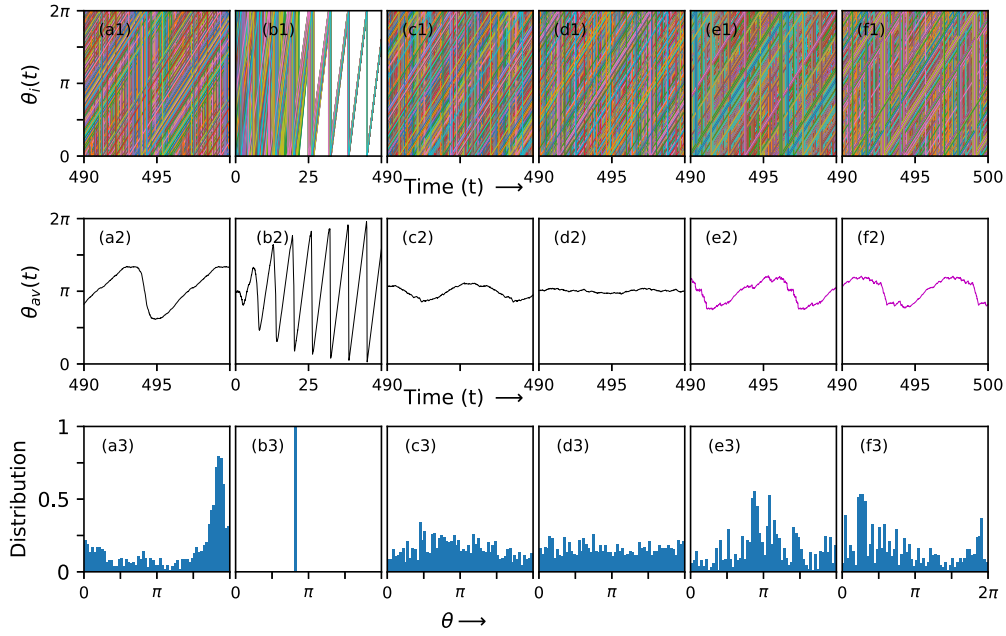

FIG. 4. Top row: Individual node's dynamics $\theta_i(t)$ vs time t in the indicated interval [final 1000 time steps, except for the pattern (b1), which is shown for the initial 1000 time steps]. The parameters $(K_1, K_2)f$, b on the forward or backward branch are set as $(-1, 0)f$, $(1, 0)b$, and $(0, 0.2)f$ for the network $\nu = 5$, corresponding to patterns (a1), (b1), and (c1), respectively; meanwhile, the patterns (d1), (e1), and (f1) are for $(-1, 0)f$, $(-1, 0)b$, and $(-1, 0.2)b$ for the sparse network with $\nu = -5$. Middle row: the network averaged phase $\theta_{\rm av}(t)$ as a function of time in the same time interval as the corresponding pattern above it. Bottom row: histogram of the node's phases θ_i taken at the end of that period corresponding to the panels in the same column above it.

respectively. Similarly, the patterns on panels (d1), (e1), and (f1) correspond to the case $(-1, 0)f$, $(-1, 0)b$, and $(-1, 0.2)b$ for the sparse network with $\nu = -5$. The middle and bottom row below each pattern shows the corresponding network's averaged phase $\theta_{\rm av}(t)$ in the same time interval, and the histogram of phases of individual nodes at the end of that time interval.

For the compact structure ($\nu = 5$), we have that the order parameter $r \approx 0.5$ at the point $(-1, 0)f$; the corresponding pattern of phases, shown in panel (a1) of Fig. 4, indicates that groups of roughly synchronized nodes are formed and evolve with the same speed. The respective average phase fluctuates in an extended range around π, as shown in panel (a2). In the distribution of the nodes' phases, in (a3), broad peaks indicate the formation of uneven groups of nodes with close but not fully synchronized phases θ_i. The situation is much different at $(-1, 0)b$ in the backward branch, where the system remains fully synchronized, corresponding to a single sharp peak in (b3). The pattern of individual phases in (b1) shows how such a synchronized state forms in time when starting from a random initial state. Consequently, the average phase in (b2) reaches the full range of values on the unit circle. The panels (c1)–(c3) show how the order parameter appears at the point $(0, 0.2)f$ under the impact of weak triangle-based coupling alone. The pattern in (c1) and the corresponding average phase in (c2) show that the network's compactness promotes ordering by forming small groups, even though the leading pairwise interaction is absent.

The phase evolution patterns are different in the sparse network ($\nu = -5$), as shown in the panels (d1)–(f1). At the point $(-1, 0)f$, the order-parameter value $r = 0.03$ appears through many small groups of (roughly) synchronized nodes, shown in (d1), corresponding to an almost even distribution of phases over the network nodes, cf. (d3), with tiny fluctuations of the average phase about π, in (d2). At the point $(-1, 0)b$ on the backward branch, the order parameter is dropped from $r = 1$ to a finite value, which is compatible with the pronounced formation of groups visible in panel (e1) and in the distribution; cf. (e3). The corresponding average phase fluctuates in a larger interval, as shown in panel (e2). A similar fluctuation range of the average phase is observed in panel (f2), corresponding to the similar value of the order parameter at the point $(-1, 0.2)b$; cf. Fig. 3. However, the presence of a weak higher-order interaction, in this case, leads to a different grouping of nodes, which is illustrated by the phase evolution pattern in panel (f1) and the phase histogram in (f3).

D. Hysteresis properties in the transition from uniform to distributed internal frequencies

To explore the impact of the distribution of internal oscillator frequencies, they are drawn from a normal distribution of the width σ centered about $\omega = 1.0$. By increasing the width of the distribution σ, we show new features of the hysteresis loop that appear, compared to the case of δ-distribution in Fig. 3, and how these features depend on the network structure. The results for the intermediate width, $\sigma = 0.01$, and a broad distribution $\sigma = 0.1$, are shown in Figs. 5 and 6, respectively.

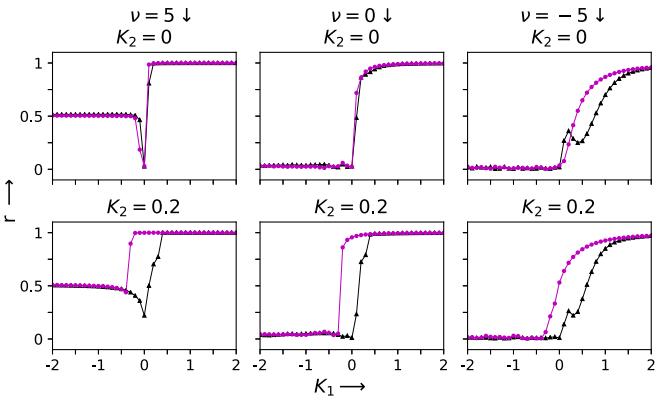

FIG. 5. Transition to synchronization and hysteresis in networks with $\nu = 5, 0, -5$ (left to right columns), where ω is drawn from a Gaussian distribution width $\sigma = 0.01$ around $\omega = 1.0$; $K_2 = 0$ (top row) and $K_2 = 0.2$ (bottom row). The solid triangles (black) and solid circles (magenta) represent the value of order parameter r in forward and backward sweeps, respectively.

Both Figs. 5 and 6 show that, in the presence of distributed internal frequencies, the partial synchronization at $K_1 < 0$ persists in all networks with the respective value of the order parameter unchanged compared to the case of δ-distribution; cf. Fig. 3. Moreover, the hysteresis loop is virtually absent unless the higher-order coupling K_2 is switched on. Remarkably lower values of K_2 are needed to induce desynchronization via an abrupt drop of the order parameter, i.e., in the compact network ($\nu = 5$) compared with the case of homogeneous internal frequencies. We also observe several new features in the forward/backward sweeps. Particularly in the compact network, a drop of the order parameter at $K_1 \leqslant 0$ occurs before it rises again to reach complete synchrony at $K_1 > 0$; see the left columns in Figs. 5 and 6. While such a drop is absent in the case of δ-distribution, the area $K_1 \lesssim 0$ where the order parameter is decreasing from the level $r = 0.5$ to zero is broadening upon increasing the frequency distribution width σ. In the sparse and mixed networks, on the other hand, the increasing spread of internal frequencies width σ makes the

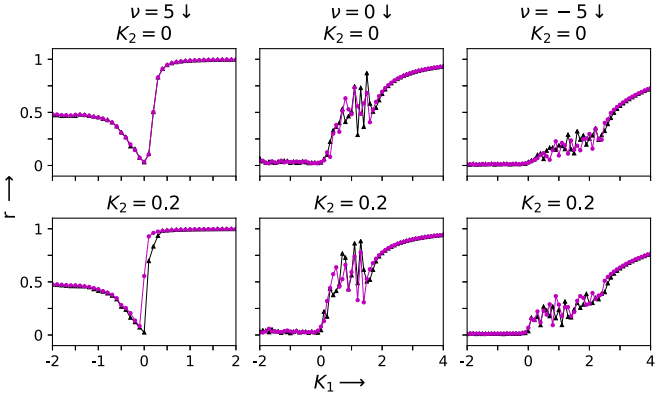

FIG. 6. Same as Fig. 5 but with the ω drawn from a Gaussian distribution with the width $\sigma = 0.1$. In the sparse network, we find that $r \to 1$ asymptotically at $K_1 \gtrsim 10$ (not shown). Note the absence of hysteresis for these values of higher-order interactions K_2.

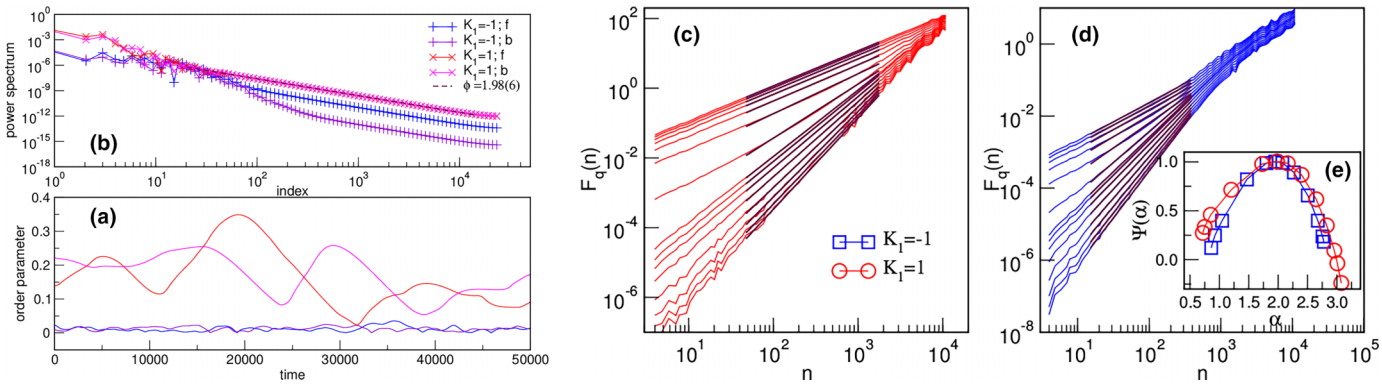

FIG. 7. In the network for $\nu = -5$, the order-parameter time series (a) and the corresponding power spectrums (b) at two points corresponding to the partial synchronization at $K_1 = -1$ and 1 on the forward (f) and backward (b) loop in the absence of higher-order coupling, $K_2 = 0$. (c), (d) The fluctuation function $F_q(n)$ vs the time interval n for the order parameter in the forward loops at $K_1 = -1$ (blue) and $K_1 = 1$ (red). Each line corresponds to different values of the amplification parameter $q \in [-3.5, 3.5]$ bottom-to-top; the scaling area is indicated by the straight lines giving the generalized Hurst exponent H_q, which leads to the corresponding singularity spectra $\Psi(\alpha)$ vs α given in panel (e).

complete synchronization (in the considered network's sizes $N = 1000$ nodes) increasingly more difficult even at very large $K_1 > 0$. For example, when $\sigma = 0.1$, the much larger pairwise coupling, $K_1 \approx 10$, is required for the order parameter to asymptotically approach $r \lesssim 1$ (not shown). Recall that we have $d_s \leqslant 2$ in these two networks, which implies unstable phase correlations with the increasing network size. Here, we observe another instability for a fixed network size by changing the weak pairwise interaction strength. Instead of a steep increase in synchrony for $K_1 \geqslant 0$, we observe a robust instability where the (time-averaged) order parameter achieves different values when the interaction strength K_1 is changed by a small amount; this feature appears both at the forward as well as the backward branch and is practically unaffected by the weak higher-order interactions; see the middle and right columns in Fig. 6. To a smaller extent, such instability is seen in the sparse network already at a smaller distribution width, $\sigma = 0.01$, where it causes a kind of hysteresis at the positive K_1 side, as shown in the top right panel of Fig. 5. We note that this feature appears in the networks where the building cliques share a single node, which is 100% in the case of the sparse network, and also present in the mixed network, but entirely absent in the compact network; cf. Fig. 1. Understanding the mechanisms of how these instabilities appear is another challenging problem. In the next section, we analyze the nature of the order-parameter fluctuations for the values of interactions in the range where the instability occurs in the sparse network.

IV. MULTIFRACTAL FLUCTUATIONS OF THE ORDER PARAMETER IN PARTIALLY SYNCHRONIZED STATES

In the partially synchronized states in all simplicial complexes, the order parameter for $K_1 < 0$ has finite but different values; the time-averaged values are lower in the sparse networks than the compact ones. Here, we study temporal fluctuations of the order parameter for fixed pairwise interaction strength. Specifically, for the assembly at $\nu = -5$ and a broad Gaussian distribution of the internal frequencies, a partial synchronization occurs at $K_1 < 0$ but also for a broad range of $K_1 > 0$, where a different degree of partial synchronization is observed, with $r \to 1$ asymptotically at very high K_1; cf. Fig. 6. We consider two representative points, $K_1 = -1$ and $+1$, in the absence of higher-order couplings. The respective time variations of the order parameter, shown in Fig. 7(a), both for forward and backward branches of the hysteresis loop, exhibit cyclical fluctuations around different average values for $K_1 < 0$ compared to $K_1 > 0$. These fluctuations lead to the exponent $\phi \sim 2$, compatible with the short-range correlations, fitted for an extended portion of the power spectrum at large frequencies; cf. Fig. 7(b). In the following, we show that these cycles are modulated, attaining higher harmonics, which are captured by the multifractal analysis.

For the analysis of the order-parameter fluctuations $r(t)$, we use detrended multifractal analysis of time series [51–53]. Hence, the profile $Y(i) = \sum_{k=1}^{i}[r(k) - \langle r\rangle]$ of the time series is divided in N_s segments of the length n. Repeating the procedure starting from the end of the time series $t = T_{\max}$, we get in total $2N_s = 2\,\mathrm{int}(T_{\max}/n)$ segments. Then, at each segment $\mu = 1, 2, \ldots, N_s$, the local trend $y_\mu(i)$ is determined by a polynomial (quadratic) fit, which allows computing the standard deviation around it as $F^2(\mu, n) = \frac{1}{n}\sum_{i=1}^{n}[Y[(\mu-1)n + i] - y_\mu(i)]^2$, and similarly, $F^2(\mu, n) = \frac{1}{n}\sum_{i=1}^{n}\{Y[N - (\mu - N_s)n + i] - y_\mu(i)\}^2$ for $\mu = N_s + 1, \ldots, 2N_s$. The fluctuation function $F_q(n)$ for the segment length n is then determined as

$$F_q(n) = \left(\frac{1}{2N_s}\sum_{\mu=1}^{2N_s}[F^2(\mu, n)]^{q/2}\right)^{1/q} \sim n^{H_q} \qquad (4)$$

for different positive and negative values of the amplification parameter q. The function is plotted against varied segment length $n \in [2, \mathrm{int}(T_{\max}/4)]$. Its power-law sections on the lines for different q are fitted to find the *generalized Hurst exponent* H_q, defined on the right-hand side of the expression (4). Notably, the case $q = 2$ reduces to the standard deviation function and corresponds to the well-known Hurst exponent.

The spectrum H_q is determined for a range of values of q for which the fluctuation function exhibits scale invariance; here, we use $q \in [-3.5, +3.5]$; see Fig. 7. Once the spectrum H_q is known, one can determine other multifractality

measures, in particular $\tau_q = qH_q - 1$, where the exponent τ_q is related to the standard (box probability) measure [52]. Then, using the Legendre transform $\Psi(\alpha) = q\alpha - \tau_q$, where $\alpha = d\tau/dq$, the time series *singularity spectrum* can be determined. A nontrivial singularity indicates different power-law singularities at different data points t of the time series, according to $|\nabla r(t,\epsilon)|_{\epsilon\to 0} \sim \epsilon^{\alpha(t)}$, with an exponent depending on the data point t [51,52]. Thus, the value $\psi(\alpha)$ stands for a fractal dimension of the time series points having the same singularity exponent α. Note that for a monofractal, $H_q = H_2 = \text{const}$, causing the spectrum $\Psi(\alpha)$ to reduce to a single point $\alpha = H_2$, where H_2 is the standard Hurst exponent.

In Figs. 7(c) and 7(d), we show the results for the fluctuation function $F_q(n)$ as a function of the time interval n for the order-parameter curves in the forward branch at $K_1 = -1$ (blue) and $K_1 = 1$ (red lines). As these figures show, in both cases the fluctuation function $F_q(n)$ exhibits a scaling region for a broad range of time intervals n. The fitted area of $F_q(n)$ for different q (indicated by thick dark lines) gives the corresponding H_q exponent defined in Eq. (4). In both cases, the resulting broad spectra H_q are transformed onto the singularity spectra $\Psi(\alpha)$, which are given in the inset, Fig. 7(e). The parabolic distribution for both spectra is asymmetrical, having a broad range of values with a maximum close to $\alpha = 2$ and somewhat different curvature. Hence, the mechanisms behind the occurrence of partial synchronization, as discussed above, are compatible with the multifractal temporal fluctuations of the order parameter with broad singularity spectra.

V. DISCUSSION AND CONCLUSIONS

We have investigated the interplay of structure, interactions, and distribution of internal frequencies in phase synchronization and desynchronization processes on four-dimensional simplicial complexes with different architecture composed of identical building blocks (5-cliques), and containing $N \geqslant 1000$ nodes; cf. Fig. 1. Of the considered structures, 5-cliques are assembled with rules of chemical affinity and geometric compatibility [15]; when chemical affinity allows the addition of the maximum number of nodes, a minimal face (a node) is shared and a sparse structure appears; oppositely, sharing the largest face (4-clique) leads to a compact assembly. For vanishing chemical affinity, a mixed structure emerges where 5-cliques can share any of their faces by geometric compatibility. The underlying graphs of these simplicial complexes are 1-hyperbolic and have different spectral dimensions [42], as shown in Fig. 2(h).

Our results suggest that these simplicial architectures enable geometric frustration effects and diverse collective dynamical phenomena. The shape of the hysteresis loop in the presence of higher-order interactions, as well as the collective fluctuations and the influence of the internal frequency distribution on the synchronization processes on these simplicial complexes, can be related to the size of shared faces by neighboring 5-cliques. This is explained more precisely as follows:

(i) Partial synchronization $r < 1$ occurs at negative pairwise coupling with a small nonzero value of the order parameter $r \sim 0.03$ found when the least shared face matches one node ($s = 1$); however, $r \sim 0.5$ when the least common face contains $s = 4$ nodes. Within numerical accuracy, these values of the global order parameter are insensitive to the internal frequency distribution and strength of triangle-based interactions.

(ii) Multiple interactions embedded in triangles change the hysteresis loop and, at a strength that differs for each simplicial complex, induce a sudden drop of the order parameter to the corresponding partial synchronization level on the negative branch of the pairwise interaction. Moreover, they prolong reaching the full synchronization with positive pairwise interactions in all simplicial complexes. This effect is particularly pronounced in the sparse architecture with distributed internal frequencies, where the state with complete synchronization (at this network size) is asymptotically approached at very large coupling strengths. Moreover, a characteristic instability of the order parameter occurs at intermediate pairwise couplings, which persists in the presence of higher-order interactions. The fully synchronized state of this structure reached at homogeneous frequencies in Fig. 3 breaks via incomplete abrupt desynchronization even without higher-order coupling. It is tempting to believe that these synchronization features can be attributed to weak phase correlations in this network structure, which is characterized by a small spectral dimension.

(iii) The evolution patterns of nodes, analyzed at selected points on the hysteresis where partial synchronization occurs, reveal coevolving groups with different phases, which leads to quasioscillatory fluctuations of the order parameter. Visually, the organization of clusters is sensitive to triangle-embedded interactions. These order-parameter fluctuations have multifractal features with broad singularity spectra associated with the simplicial structure and the interaction strength.

These findings shed new light on the nature of phase synchronization in high-dimensional simplicial complexes of different architectures in the interplay with coupling strengths and internal frequency distribution that can be relevant to many complex systems. It should be noted that a specific real system of a similar structure is represented by a fixed network and a "coupling function" between dynamical units across the link, captured by the parameter K_1. It can vary with time or some external parameters (similar to the temperature in physical laboratory spin systems, where with the fixed interaction J, the relevant parameter $K_1 \equiv J/k_BT$ is systematically driven by temperature); the range of time variations of coupling functions, e.g., in biological systems, can be determined from additional data and their impact on the synchronization transition determined; see, e.g., Ref. [54] for a study of neural coupling functions. Alternatively, both the network and the coupling function can be fixed, in which case the system's parameters correspond to a single point on the hysteresis loop. Then the analysis of the temporal evolution of phases of individual oscillators and groups of these oscillators and the combined phase or the order-parameter fluctuations (as presented in Figs. 4 and 7) describes that system's behavior.

While the transition to synchronization induced by positive pairwise interactions was much investigated [1], the nature of partial order associated with negative interactions remains to be better understood. In this regard, our simplicial complexes built of identical blocks as four-dimensional cliques present a potential for studying the complexity of synchro-

nization/desynchronization processes in greater detail beyond the measure of the spectral dimension. For example, studying the eigenvector localization [40] can reveal what mesoscopic structures are involved and the role of the nodes' correlations [36,37] in the collective dynamics. We note that these networks have assortative correlations of nodes [36]; however, there are no pronounced hubs in the sparse network; see Fig. 1. Therefore, we expect to detect the appearance of concurrent groups of nodes that cause the observed swings in the order parameter in the sparse network at weak positive couplings. Moreover, the influence of even/odd numbers of nodes in the shared faces and the geometry-embedded fourth- and fifth-order interactions remain open questions for future study. We have investigated the leading pairwise and triangle-embedded interactions that, theoretically, are responsible for the synchronization transition; however, having a finite network and hidden combinatorial geometry, we note that the increasing structural complexity correlates with the growing number of simplexes of all orders; cf. Fig. 2(g). Therefore, we expect that a competition between the pairwise interactions with simplex-embedded third-, fourth-, and fifth-order interactions may differ significantly depending on the simplicial architecture. These studies will be reported elsewhere. The results presented here reveal the simplicial architecture and coupling strengths behind dynamic states with partial synchronization, which are often desirable in complex functional systems, e.g., the brain, and ways to construct simplicial complexes of the same order that support full synchronization when needed.

ACKNOWLEDGMENTS

B.T. acknowledge the financial support from the Slovenian Research Agency under the program P1-0044. S.S. acknowledges the financial support from IC&SR, IITM through the project SB20210838AMMHRD008291. N.G. thanks IC&SR, IITM for the financial support through the project SP20210777DRMHRDDIRIIT.

[1] S. Boccaletti, P. De Lellis, C. I. del Genio, K. Alfaro-Bittner, R. Criado, S. Jalan, and M. Romance, The structure and dynamics of networks with higher order interactions, Phys. Rep. **1018**, 1 (2023).

[2] M. Boguñá, I. Bonamassa, M. De Domenico, S. Havlin, D. Krioukov, and M. Ángeles Serrano, Network geometry, Nat. Rev. Phys. **3**, 114 (2021).

[3] S. Majhi, M. Perc, and D. Ghosh, Dynamics on higher-order networks: A review, J. R. Soc. Interface **19**, 188 (2022).

[4] A. E. Sizemore, C. Giusti, A. Kahn, and J. M. Vettel, Cliques and cavities in human connectome, J. Comput. Neurosci. **44**, 115 (2018).

[5] B. Tadić, M. Andjelković, and R. Melnik, Functional geometry of human connectomes, Sci. Rep. **9**, 12060 (2019).

[6] M. Andjelković, B. Tadić, and R. Melnik, The topology of higher-order complexes associated with brain hubs in human connectomes, Sci. Rep. **10**, 17320 (2020).

[7] R. Herzog, F. E. Rosas, R. Whelan, S. Fittipaldi, H. Santamaria-Garcia, J. Cruzat *et al.*, Genuine high-order interactions in brain networks and neurodegeneration, Neurobiol. Dis. **175**, 105918 (2022).

[8] J. Y. Jung, L. L. Cloutman, R. J. Binney, and M. A. Lambon Ralph, The structural connectivity of higher order association cortices reflects human functional brain networks, Cortex **97**, 221 (2017).

[9] C. Seguin, S. Mansour L, O. Sporns, A. Zalesky, and F. Calamante, Network communication models narrow the gap between the modular organization of structural and functional brain networks, NeuroImage **257**, 119323 (2022).

[10] M. Andjelković, B. Tadić, S. Maletić, and M. Rajković, Hierarchical sequencing of online social graphs, Physica A **436**, 582 (2015).

[11] B. Tadić, M. Andjelković, B. M. Boshkoska, and Z. Levnajić, Algebraic topology of multi-brain connectivity networks reveals dissimilarity in functional patterns during spoken communications, PLoS ONE **11**, e0166787 (2016).

[12] M. Andjelković, B. Tadić, M. Mitrović Dankulov, M. Rajković, and R. Melnik, Topology of innovation spaces in the knowledge networks emerging through questions-and-answers, PLoS ONE **11**, e0154655 (2016).

[13] U. Alvarez-Rodriguez, F. Battiston, G. F. Arruda, Y. Moreno, M. Perc, and V. Latora, Evolutionary dynamics of higher-order interactions in social networks, Nat. Hum. Behav. **5**, 586 (2021).

[14] S. Ikeda and M. Kotani, Materials inspired by mathematics, Sci. Technol. Adv. Mater. **17**, 253 (2016).

[15] M. Šuvakov, M. Andjelković, and B. Tadić, Hidden geometries in networks arising from cooperative self-assembly, Sci. Rep. **8**, 1987 (2018).

[16] B. Tadić, M. Šuvakov, M. Andjelković, and G. J. Rodgers, Large-scale influence of defect bonds in geometrically constrained self-assembly, Phys. Rev. E **102**, 032307 (2020).

[17] D. Kozlov, *Combinatorial Algebraic Topology*, Springer Series Algorithms and Computation in Mathematics Vol. 21 (Springer-Verlag, Berlin, 2008).

[18] J. H. Johnson, Some structures and notation of Q-analysis, Environ. Planning B **8**, 73 (1981).

[19] B. Tadić and R. Melnik, Self-organised critical dynamics as a key to fundamental features of complexity in physical, biological, and social networks, Dynamics **1**, 181 (2021).

[20] S. Boettcher and C. T. Brunson, Renormalization group for critical phenomena in complex networks, Front. Physio. **2**, 102 (2011).

[21] M. Castellana and G. Parisi, Renormalization group computation of the critical exponents of hierarchical spin glasses, Phys. Rev. E **82**, 040105(R) (2010).

[22] A. Arenas, W. Cota, J. Gómez-Gardeñes, S. Gómez, C. Granell, J. T. Matamalas, D. Soriano-Panos, and B. Steinegger, Modeling the Spatiotemporal Epidemic Spreading of COVID-19 and the Impact of Mobility and Social Distancing Interventions, Phys. Rev. X **10**, 041055 (2020).

[23] A. Tlaie, I. Leyva, and I. Sendinna-Nadal, Higher-order couplings in geometric complex networks of neurons, Phys. Rev. E **100**, 052305 (2019).

[24] L. Ramlow, J. Sawicki, A. Zakharova, J. Hlinka, J. Christian Claussen, and E. Schöll, Partial synchronization in

empirical brain networks as a model for unihemispheric sleep, Europhys. Lett. **126**, 50007 (2019).
[25] F. Mila, Frustrated spin systems, in *Many-Body Physics: From Kondo to Hubbard*, edited by E. Pavarini, E. Koch, and P. Coleman (Forschungszentrum Jülich, Jülich, 2015), Vol. 5.
[26] B. Tadić, M. Andjelković, M. Šuvakov, and G. J. Rodgers, Magnetisation processes in geometrically frustrated spin networks with self-assembled cliques, Entropy **22**, 336 (2020).
[27] B. Tadić and N. Gupte, Hidden geometry and dynamics of complex networks: Spin reversal in nanoassemblies with pairwise and triangle-based interactions, Europhys. Lett. **132**, 60008 (2020).
[28] J. Fell and N. Axmacher, The role of phase synchronization in memory processes, Nat. Rev. Neurosci. **12**, 105 (2011).
[29] L. Gollo and M. Breakspear, The frustrated brain: from dynamics on motifs to communities and networks, Philos. Trans. R. Soc. B **369**, 20130532 (2014).
[30] F. A. Rodrigues, T. Peron, P. Ji, and J. Kurths, The kuramoto model in complex networks, Phys. Rep. **610**, 1 (2016).
[31] S. Dutta, P. Kundu, P. Khanra, C. Hens, and P. Pal, Perfect synchronization in complex networks with higher-order interactions, Phys. Rep. E **108**, 024304 (2023).
[32] T. Carletti, L. Giambagli, and G. Bianconi, Global Topological Synchronization on Simplicial and Cell Complexes, Phys. Rev. Lett. **130**, 187401 (2023).
[33] P. S. Skardal and A. Arenas, Higher order interactions in complex networks of phase oscillators promote abrupt synchronization switching, Commun. Phys. **3**, 218 (2020).
[34] R. Ghorbanchian, J. Restrepo, J. J. Torres, and G. Bianconi, Higher-order simplicial synchronization of coupled topological signals, Commun. Phys. **4**, 120 (2021).
[35] K. Kovalenko *et al.*, Growing scale-free simplices, Commun. Phys. **4**, 43 (2021).
[36] M. Chutani, B. Tadić, and N. Gupte, Hysteresis and synchronization processes of kuramoto oscillators on high-dimensional simplicial complexes with competing simplex-encoded couplings, Phys. Rev. E **104**, 034206 (2021).
[37] B. Tadić, M. Chutani, and N. Gupte, Multiscale fractality in partial phase synchronisation on simplicial complexes around brain hubs, Chaos, Solitons Fractals **160**, 112201 (2022).
[38] A. P. Millán, J. J. Torres, and G. Bianconi, Synchronization in network geometries with finite spectral dimension, Phys. Rev. E **99**, 022307 (2019).
[39] M. Khoshkhou and A. Montakhab, Explosive, continuous and frustrated synchronization transition in spiking Hodgkin–Huxley neural networks: The role of topology and synaptic interaction, Physica D **405**, 132399 (2020).
[40] M. Mitrović and B. Tadić, Spectral and dynamical properties in classes of sparse networks with mesoscopic inhomogeneities, Phys. Rev. E **80**, 026123 (2009).
[41] C. Castellano and R. Pastor-Satorras, Relating Topological Determinants of Complex Networks to Their Spectral Properties: Structural and Dynamical Effects, Phys. Rev. X **7**, 041024 (2017).
[42] M. Mitrović Dankulov, B. Tadić, and R. Melnik, Spectral properties of hyperbolic networks with tunable aggregation of simplexes, Phys. Rev. E **100**, 012309 (2019).
[43] A. P. Milan, J. J. Torres, and G. Bianconi, Complex network geometry and frustrated synchronization, Sci. Rep. **8**, 9910 (2018).
[44] D. Horak and J. Jost, Spectra of combinatorial laplace operators on simplicial complexes, Adv. Math. **244**, 303 (2013).
[45] M. Šuvakov, M. Andjelković, and B. Tadić, Applet: Simplex aggregated growing graph, http://suki.ipb.rs/ggraph/ (2017).
[46] S. Samanta, P. Raval, R. G. N. Manjurata, and C. Debangshu, Cooperative self-assembly driven by multiple noncovalent interactions: Investigating molecular origin and reassessing characterization, ACS Cent. Sci. **7**, 1391 (2021).
[47] S. Bermudo, J. M. Rodríguez, J. M. Sigarreta, and J.-M. Vilaire, Gromov hyperbolic graphs, Discrete Math. **313**, 1575 (2013).
[48] N. Cohen, D. Coudert, G. Ducoffe, and A. Lancin, Applying clique-decomposition for computing gromov hyperbolicity, Theor. Comput. Sci. **690**, 114 (2017).
[49] P. Virtanen, R. Gommers, T. E. Oliphant, M. Haberland, T. Reddy *et al.*, SciPy 1.0: Fundamental algorithms for scientific computing in python, Nat. Methods **17**, 261 (2020).
[50] A. Roy and N. Gupte, The transition to synchronization on branching hierarchical lattices, Chaos **32**, 013120 (2022).
[51] A. N. Pavlov and V. S. Anishchenko, Multifractal analysis of complex sisgnals, Phys. Usp. **50**, 819 (2007).
[52] J. W. Kantelhardt *et al.*, Multifractal detrended fluctuation analysis of nonstationary time series, Physica A **316**, 87 (2002).
[53] B. Tadić, Multifractal analysis of Barkhausen noise reveals the dynamic nature of criticality at hysteresis loop, J. Stat. Mech. (2016) 063305.
[54] Z. Hugos, T. Stankovski, J. Newman, T. Pereira, P. V. E. McClintock and A. Stefanovska, Synchronization transitions caused by time-varying coupling functions, Philos. Trans. R. Soc. A. **377**, 20190275 (2019).